Available online at www.sciencedirect.com

ScienceDirect

Proceedings of the Combustion Institute 35 (2015) 3537–3545

Proceedings of the Combustion Institute

www.elsevier.com/locate/proci

Visualization of MILD combustion from jets in cross-flow

J. Sidey *, E. Mastorakos

Hopkinson Laboratory, Engineering Department, University of Cambridge, UK

Available online 2 August 2014

Abstract

The behaviour of methane jet flames autoigniting in a turbulent cross-flow at MILD combustion conditions was examined experimentally. The methane jet was injected orthogonally into a turbulent, low oxygen ($X_{O2x} < 8\%$) cross-flow at high temperatures in a cylindrical quartz tube. Regardless of cross-flow conditions, the methane jet autoignited and a flame was stabilized in a wide region clearly separated from the injection nozzle. OH^* chemiluminescence images show that OH^* intensity was not significantly diminished by changing X_{O2x}, but the size of the reacting region, as well as its location, was noticeably sensitive to X_{O2x}. Cross-flows enriched with additional air sustained methane jet flames with larger reactive regions than those diluted with N_2 or composed of pure hot products. Additional cross-flow dilution with N_2 shifted the reaction further downstream, an observation supported by the imaging of individual autoignition kernels. Mean OH-PLIF shows OH radical presence in areas devoid of heat release, as indicated by the time-averaged OH^* chemiluminescence images. In all cases, OH-PLIF instantaneous images show regions with wide OH distributions, but sharp gradients, similar to those evident in traditional combustion regimes. The data interpretation is supported by laminar non-premixed flame calculations that demonstrate some differences and similarities between MILD and conventional flames.

Keywords: Jet-in-cross-flow; Autoignition; Hot products; MILD combustion

1. Introduction

A fuel jet injected into an oxidiser co-flow has been widely studied. For the Moderate or Intense Low oxygen Dilution (MILD) regime [1], where the co-flow is oxygen-deficient and hot, fuel jets in parallel-flowing vitiated air have been studied with emphasis on pollutant suppression, flame stabilisation, autoignition, and flame structure [2–7]. The formation of autoignition kernels and their statistics in hot air [8] and diluted [9] co-flows was studied to reveal the effect of co-flow temperature, velocity, and Reynolds number on autoignition location and kernel appearance frequency.

While significant progress on jet flames in heated or diluted co-flows has been made, configurations involving transverse jets in similar condition cross-flows remain little studied. Hasselbrink and Mungal [10,11] studied lifted flames in cold

* Corresponding author. Address: Department of Engineering, University of Cambridge, Trumpington Street, Cambridge CB2 1PZ, UK. Fax: +44 1223 339906.

E-mail address: jams4@cam.ac.uk (J. Sidey).

http://dx.doi.org/10.1016/j.proci.2014.07.028
1540-7489/

air cross-flows in detail, developing scaling methods for predicting transverse jet vortical systems and commenting on the interaction between heat release and flow properties. A review paper is also available [12]. More recently, a DNS study of autoigniting diluted fuel jets in heated cross-flows was performed and it was found that the resulting jet flame stabilizes in a near stoichiometric, low velocity region between the jet's large counter-rotating vortices [13]. Micka and Driscoll [14] experimentally studied jet flames in a high-speed preheated air cross-flow. Through CH, OH, and CH_2O imaging they identified a lift-off region upstream of the flame front in which autoignition radicals are formed in significant quantities, a finding consistent with previous work [3,5,6]. Through the identification of spatially wide regions with pre-ignition species and considering their high cross-flow temperature, Micka and Driscoll determined that their jet flame was autoignition-controlled, while mixing between the jet and cross-flow was cross-flow-velocity controlled [10,11]. The relationship between autoignition delay time and oxygen mole fraction under diluted conditions for liquid fuels, particularly relevant for diesel applications, has been addressed in Ref. [15].

Although the above links the concept of autoignition-controlled stabilisation with the jet-in-cross-flow geometry, the effects of coupled cross-flow dilution and preheat, which is relevant to MILD combustion, have not been investigated explicitly. Furthermore, the balance between stabilisation, prominent in cases involving combustion of jets in cold air, and autoignition, prominent in cases involving combustion of jets in hot oxidiser, is still not well understood. An understanding of the stabilisation mechanisms of jets in diluted and preheated co- and cross-flows is particularly important when considering the transition between conventional and MILD combustion regimes in practical systems. This paper aims to address this problem by examining methane jet flames in oxygen-deprived hot cross-flows. The experiment can also be thought of as a fundamental study of a geometrical feature present in various practical realisations of MILD combustion where jets are introduced at various angles relative to the hot product flow [16,17].

2. Method

The experimental apparatus (Fig. 1) was operated at atmospheric pressure. It consisted of a premixed burner base and a 350 mm quartz tube. Methane and air were premixed through the cylindrical base to establish a flat, blue, premixed flame on an alumina foam downstream of a perforated plate and a flashback arrestor. The burnt gases from this premixed flame then pass through an

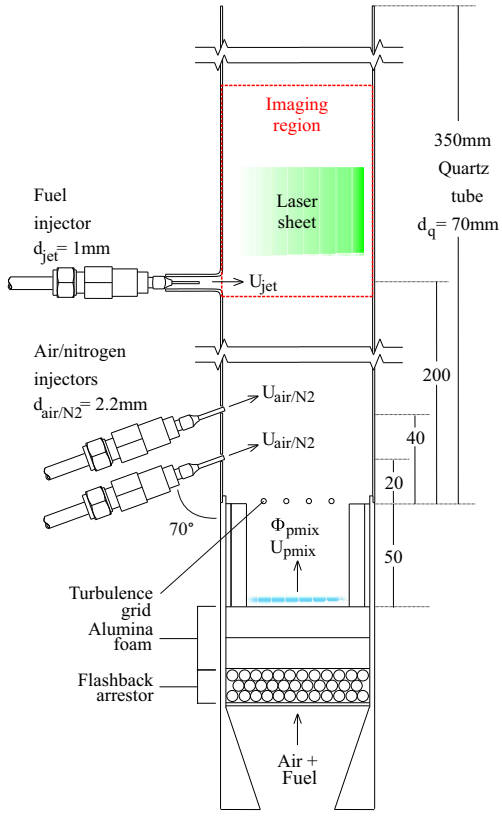

Fig. 1. A schematic of the experimental apparatus.

alumina turbulence grid of 2 mm diameter rods with a blockage ratio of 0.18 and mesh size of 8 mm. Downstream of the grid, air or N_2 was injected from two $d_{air/N2} = 2.2$ mm inlets arranged 70° from the cross-flow direction. Preliminary measurements of oxygen content across the tube indicated that the air or N_2 and hot products are well mixed 200 mm downstream of the turbulence grid, the axial location of the perpendicular $d_{jet} = 1$ mm fuel injector. Cross-flows of various composition, summarised in the upper portion of Table 1, were tested to isolate the effects of temperature, velocity, and oxygen content on the CH_4 jet flame's structure. Three cross-flow condition subsets were considered: (a) hot products from a premixed flame of known equivalence ratio (Φ_{pmix}), (b) hot products mixed with cold air (at velocity U_{air} through each air/N_2 injector), and (c) hot products mixed with cold N_2 (U_{N2} through each air/N_2 injector). Each cross-flow condition detailed in Table 1 and assigned a case identifier indicating Φ_{pmix}, hot product velocity estimated from the cold flow rate and the adiabatic flame temperature (U_{pmix}), U_{air}, and U_{N2}. Assuming the cross-flow is fully mixed, these flow variables allow for the calculation of estimated overall cross-flow velocity, U_x, temperature (with hot

Table 1
Cross-flow (top) and fuel jet (bottom) conditions.

Case	Φ_{pmix}	U_{pmix} (m/s)	U_{air}	U_{N2}	U_x	T_x (K)	X_{O2x}
06	0.6	4.36	–	–	2.22	1665	7.8%
07	0.7	4.89	–	–	2.50	1838	5.7%
08	0.8	5.41	–	–	2.76	1997	3.7%
07A1	0.7	4.89	27	–	1.86	1374	7.7%
07A2	0.7	4.89	32	–	1.78	1313	8.1%
07A3	0.7	4.89	35	–	1.74	1285	8.3%
07A4	0.7	4.89	38	–	1.70	1259	8.5%
07A5	0.7	4.89	41	–	1.67	1234	8.7%
07N1	0.7	4.89	–	27	1.86	1374	5.7%
07N3	0.7	4.89	–	35	1.74	1285	5.7%
07N5	0.7	4.89	–	41	1.67	1234	5.7%

Suffix	U_{jet} (m/s)	Re_{jet}
F1	30	1914
F2	78	5008
F3	126	8050

gases from the premixed flame considered to be at the premixed flame's adiabatic temperature), T_x, and oxygen mole fraction, X_{O2x}. Cross-flow temperature was measured, although is not reported here due to the high error arising from the radiation of both the thermocouple and alumina grid. The described cross-flow conditions may be considered MILD by the regime markers stipulated by both Dally et al. [2] ($Y_{O2} < 9\%$) and Cavaliere and de Joannon [1] (a preheat temperature above an autoignition threshold and a relatively small temperature rise during combustion).

Three fuel jet conditions (denoted with a suffix F1, F2, or F3 on each cross-flow case identifier) correspond to a fuel jet velocity (U_{jet}) of 30, 78, and 126 m/s, respectively (Table 1). Notation pairing a cross-flow condition with a fuel velocity suffix will be used to identify each experiment. For example, a case involving a $U_{jet} = 78$ m/s CH_4 jet burning in a cross-flow of hot products from a $\Phi_{pmix} = 0.7$ flame and N_2 ($U_{N2} = 35$ m/s from each air/N_2 injector), would be identified as 07N3F2. Overall equivalence ratio, denoted as Φ, including $U_{pmix}, U_{air/N2}$, and U_{jet} can be calculated and is presented in the results.

Fast (5 kHz) OH^* chemiluminescence and OH-PLIF imaging were used to study jet flame structure under each fuel and cross-flow condition. The imaging equipment and techniques used in this study have been presented previously [18,19]. Note, however, that the OH^* chemiluminescence imaging presented here required a very high intensifier gain compared to that necessary to image lean premixed flames ($\Phi = 0.64$) [18], implying a much weaker chemiluminescence emission from MILD flames. No such gain adjustment was required for OH-PLIF measurements. Mean and instantaneous OH^* chemiluminescence and OH-PLIF images are presented with a frame size corresponding to the walls of the quartz tube. A solid red line on the bottom left of each image denotes the axial location of fuel injection. Mean images were created by averaging frames taken over 1 s while laser sheet inhomogeneities were corrected with a Gaussian intensity profile.

For some cross-flow and jet condition combinations, jet trajectories were estimated using the correlation $y = Ard_{jet}(x/rd_{jet})^B$ where $r = \left(\rho_{jet}U_{jet}^2/\rho_x U_x^2\right)^{1/2}$ [20]. A and B are constants which are often assigned values of $A = 2.05$ and $B = 0.28$, although most reported values lie between the ranges $1.2 < A < 2.6$ and $0.28 < B < 0.34$ [10]. Here, the trajectory has been calculated using the upper and lower limits of the constants A and B (solid red lines in Fig. 3; discussed later) and the most often accepted values for A and B (2.05 and 0.28 respectively; dashed white line Fig. 3).

Finally, laminar counterflow diffusion flame calculations were performed in COSILAB [21] to support the experimental findings. Two cases were examined: (a) cold CH_4/air at various strain rates and (b) cold CH_4 against equilibrium hot products of lean premixed flames ($\Phi_{pmix} = 0.6$, 0.7, and 0.8). The $\Phi_{pmix} = 0.6, 0.7$, and 0.8 hot combustion products had an initial OH mole fraction, X_{OH}, of 2.31×10^{-4}, 7.34×10^{-4}, and 1.63×10^{-3}, respectively. All simulations were performed at atmospheric pressure with the GRI-3.0 mechanism [22], supplemented by the OH^* and CH^* sub-mechanisms presented by Panoutsos et al. [23]. The inclusion OH and CH chemiluminescent species in the chemical mechanism was performed to aid the comparison and understanding of OH-PLIF and OH^*

chemiluminescence experimental results. The mechanism, evaluated in comparison with premixed and non-premixed methane-air flames, [23] utilises excited species OH^* and CH^* rate constants from Carl et al. [24] and Elsamra et al. [25] and collusional quenching data from Tamura et al. [26].

3. Results and discussion

3.1. Observations

In all experiments, the injected fuel autoignited and stabilized as a turbulent and bent jet flame without an external ignition source. Because the burning jets emitted very little light, direct photographs convey very little information. Depending on the oxygen content, X_{O2x}, and temperature, T_x, of the cross-flow, the fuel jet would either ignite and stabilize as a connected flame (usually characteristic of the higher X_{O2x} cross-flows, such as those with injected air) or ignite in patches (characteristic of lower temperature cross-flows diluted with N_2). Therefore, the experiment operates within an autoignition regime and at conditions necessary for MILD combustion [2,1].

3.2. OH^* chemiluminescence mean images

Mean OH^* chemiluminescence results of jets in $\Phi_{pmix} = 0.6, 0.7,$ and 0.8 hot product cross-flows are shown in Fig. 2. Each image shows a reaction region of comparable intensity varying in size and location within the quartz reaction tube. The cross-flow produced by the leanest premixed flame (lowest temperature, T_x, highest oxygen, X_{O2x}, containing only the hot products of the $\Phi_{pmix} = 0.6$ flame) supports a slim reaction zone with a large region of intense heat release, shown in the top row of Fig. 2. As Φ_{pmix} becomes richer, the region of high OH^* diminishes slightly in size, evident from the comparison of the 06F1 with the 07F1 and 08F1 flames. Despite this, the overall OH^* intensity and size of the reaction zone remains unchanged, although the latter broadens slightly, perhaps as a result of a higher U_x. Furthermore, a dark region, marked by the white dashed line in the $\Phi_{pmix} = 0.7$ and 0.8 cases, is evident and more prominent in experiments with richer overall equivalence ratios, Φ. The absence of reaction near the nozzle is typical of lifted flames in cold [11] or hot oxidiser [5,6,3,14] and, for the latter, it is attributed to the build-up of pre-ignition intermediates. Under all examined cross-flow conditions, as U_{jet} increases from 30 to 126 m/s from left to right in Fig. 2, the CH_4 jet flame begins to impinge on the opposite wall of the quartz tube, further dispersing the reaction zone and causing the jet to recirculate outwards along the walls of the quartz.

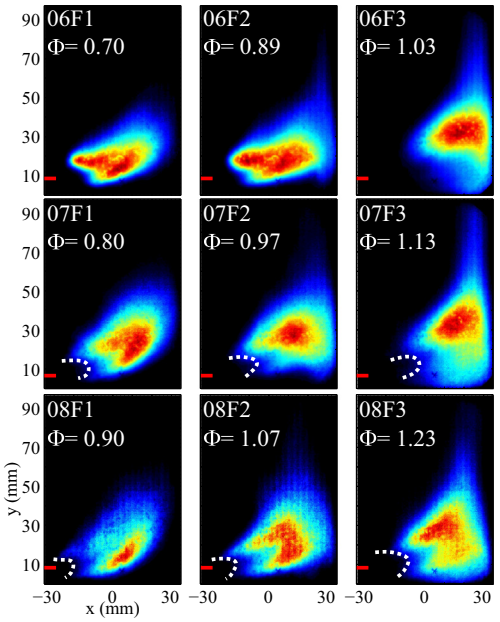

Fig. 2. Mean OH^* chemiluminescence images of CH_4 jet flames in hot product cross-flows generated by premixed flames with $\Phi_{pmix} = 0.6, 0.7,$ and 0.8. Including the fuel injected, the global equivalence ratio, Φ is also shown.

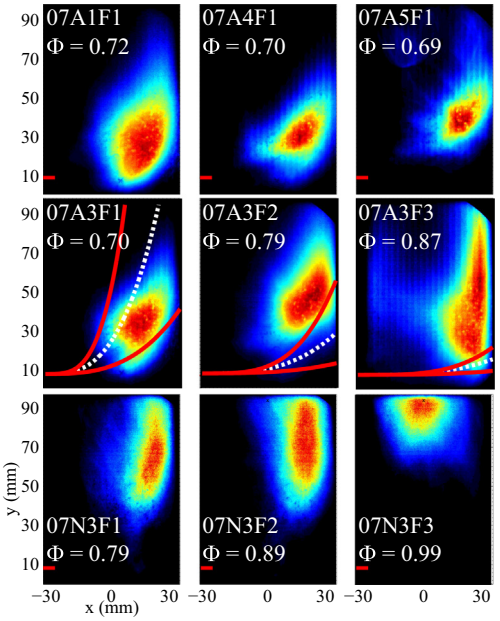

Fig. 3. Mean OH^* chemiluminescence images of CH_4 jet flames in turbulent hot product/air or hot product/N_2 cross-flows. Notation as in Fig. 2.

The first two rows of Fig. 3 show mean OH^* chemiluminescence images with hot product/air cross-flows. The addition of air through the two jets above the premixed flame has three primary

effects: (i) an increased Reynolds number, (ii) decreased temperature, and (iii) increased oxygen content. The addition of oxygen to the cross-flow, in comparison with the hot product cross-flow case at a comparable Φ_{pmix}, 07F1, increases both the size of the overall reaction zone and the high intensity heat release region of that reaction zone. As U_{air} in each oxidizer injector increased from 27 to 38 and 41 m/s - a transition visible through 07A1F1, 07A4F1, and 07A5F1 images on the top row of Fig. 3 - the high intensity reaction zone size decreases while the location of the reaction zone moves downstream in the quartz tube. Another appreciable difference arises when the fuel flow rate increases, exemplified by 07A3F1, 07A3F2, and 07A3F3 mean images in the second row of Fig. 3; higher velocity CH_4 jets burn with a larger reaction zone and, eventually, impinge on the far quartz wall (similar to the 07F3 and 08F3 cases), causing a further widening of the reacting region. Lines indicating estimated jet centreline trajectories for 07A3F1, 07A3F2, and 07A3F3 flames are indicated on the respective mean images. Taking into account that the higher fuel velocity flames, 07A3F2 and 07A3F3, impinge on the wall of the quartz tube, we do not expect the flame to lie along the trajectory. In contrast, the 07A3F1 flame's peak OH^* intensity lies between the estimates.

The bottom row of Fig. 3 shows mean OH^* chemiluminescence images of jets in N_2-diluted hot products, which are presumably very close in both temperature and fluid mechanical properties, but with significantly less oxygen, compared to supplementing with air. These images show that, while a lack of available X_{O2x} has decreased the intensity of the heat release in the hot product/air cross-flow jet flames, it has also caused the reaction zone to shift downstream relative to the corresponding hot product/air flame. When comparing these time-averaged jets with the trajectories estimated in the row above (note that the same trajectories calculated for air are relevant for each N_2 diluted cross-flow as the two cases differ only in X_{O2x}), it seems that jets burned in a cross-flow with less available oxygen tend to match more closely with conservative, or lower limit, trajectories. While it is difficult to comment conclusively on jet trajectories involving higher velocity fuel jets due to interference of the quartz wall, it should be noted that CH_4 jets in N_2 diluted cross-flows burn further downstream than those in respective air enriched cross-flows. This observation that the fuel jet autoignites further downstream in low X_{O2x} is supported by empirical observations of kernel formations in both air enhanced and N_2 diluted hot product cross-flow cases.

3.3. Kernel formation

Figure 4 illustrates two typical autoignition sequences in similar air/hot product (top) and N_2/hot product (bottom) cross-flow conditions. In both cases, kernels evolve from a dark background and spread, expanding through the jet-cross-flow mixture, until either extinguishing before the development and propagation of a new kernel or stabilizing as a flame with a wide reaction zone. In the air enhanced cross-flow, a small OH^* heat release zone appears as a well-defined and thin reactive region near the axis of the fuel jet. It quickly expands in thin fronts. In the N_2-diluted cross-flow, the kernel forms further downstream, by about 50 mm, than in the air enriched cross-flow. Further, the kernel reaction front is more dispersed and grows more slowly. After the same amount of time, the developed kernel in the N_2-diluted cross-flow fills just over half of the imaging area than that in the air-enriched

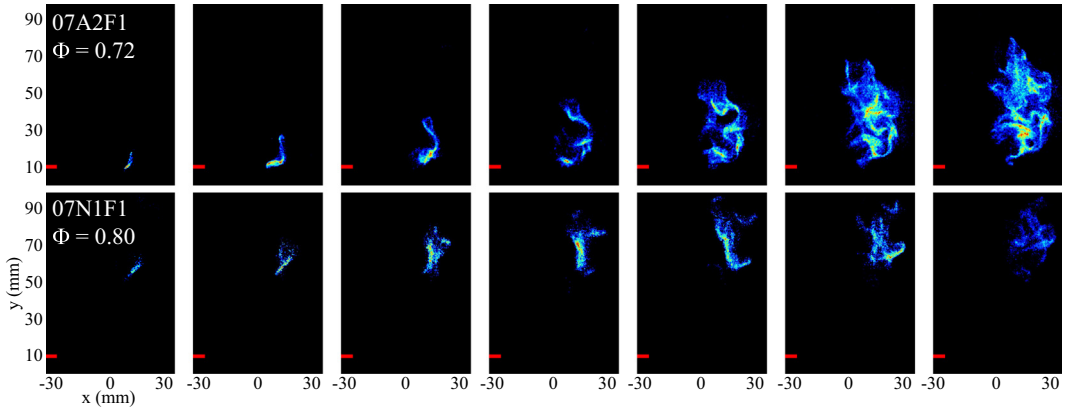

Fig. 4. Instantaneous OH^* chemiluminescence images for air enriched (top) and N_2 diluted (bottom) cross-flows. Frames show 2 ms increments.

flow. Slower chemistry resulting from dilution with an inert species agrees with counterflow diffusion flame calculations [27]. Cross-flows diluted with N_2 consistently stabilized relatively slower-growing lifted flames further downstream than cross-flows of similar temperature and velocity but higher oxygen contents.

3.4. OH-PLIF mean and instantaneous images

OH-PLIF mean images of cases 07F1–3 and 08F1–3 are shown in Fig. 5. The size of the mean OH region is generally consistent with the corresponding mean OH^* chemiluminescence image, with a few notable exceptions. Regions outlined in white draw attention to areas where OH-PLIF signal indicates clear OH presence while, by comparison, OH^* chemiluminescence indicates little or no heat release in the same location. The mismatch of areas of heat release and OH radical presence is an unusual observation as, in conventional non-premixed combustion processes, OH existence should correspond well with areas of significant heat release. This may be an identifiable feature of heavily diluted, or MILD, combustion and is explained by laminar flame calculations later.

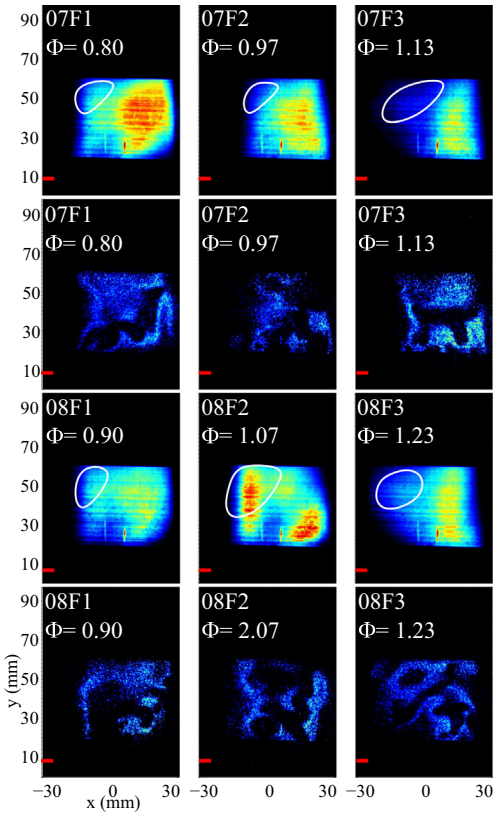

Fig. 5. Mean (first and third row from the top) and instantaneous OH-PLIF images of CH_4 jets in hot product cross-flows. Notation as for Fig. 2.

Instantaneous images are presented in Fig. 5 below each mean image of the condition to which they correspond. Dark regions within the laser sheet profile are likely to indicate areas of rich mixture or cross-flow fluid that is free of detectable OH. In each experimental case, these regions transition with a sharp gradient over what can be identified as a flame front to an intermediate or high intensity region of burned or burning gases. This clearly-defined flame front is visible in all experimental cases, indicating that, regardless of temperature and oxygen content, the reaction contains thin fronts. This is consistent with previous results regarding autoignition in air [8] and hot products [9].

Figure 6 shows instantaneous OH-PLIF frames of a 07A1F1 flame, each taken 10 ms from the last. These images further support the conclusion that, while burning in a MILD cross-flow, CH_4 jets burn in thin, distinct regions rather than cloudy or dispersed fronts as could have been hypothesised from the regime's luminosity characteristics. In each frame, sharp gradients marking transitions between regions with OH and without are visible. In particular, the 40 ms frame clearly shows a dark region, likely associated with the bent jet core forced upwards by the quartz wall, flanked on either side by thin regions with considerable concentrations of OH. Other studies, investigating OH-PLIF of jets in MILD co-flow, also identify the presence of these thin OH zones, however, they observe a thickening of these zones as available co-flow oxygen decreases [3]. In a heated, high velocity air cross-flow, jets were

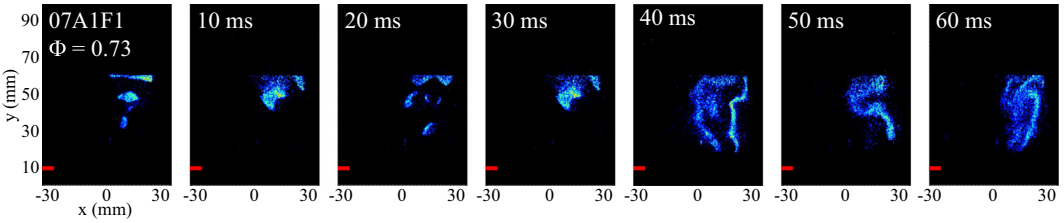

Fig. 6. Instantaneous OH-PLIF images of a CH_4 jet in a hot product/air cross-flow.

observed to burn in discrete regions of OH and CH, with CH imaging indicating the presence of "thickened" CH radical regions [14]. In this study, OH-PLIF did not indicate significant differences in the appearance or thickness of high OH radical concentration regions between cross-flows of varying oxygen content. The present observation that MILD combustion flames contain thin OH fronts is consistent with that of a recent DNS study [28].

3.5. Laminar non-premixed flame calculations

Observations arising from the analysis of the OH-PLIF experimental results presented here are supported by laminar diffusion flame calculations in Fig. 7. For the CH_4/air flames, the strain rate varied from $a = 50$ to $150\ s^{-1}$. These non-premixed flames burn at a mixture fraction between 0.05 and 0.10, marked by peaks in temperature (top), and OH mole fraction (X_{OH}, middle), and OH^* emission mole fraction (X_{OH*}, bottom). The regions of significant OH^* emission lie inside only slightly wider OH radical regions in mixture fraction space. In addition to these conventional flames, three cases relevant to the reported cross-flow experiment are presented. In each of these cases, hereafter referred to as diluted, the oxidizer was hot products from a premixed flame with the reported equivalence ratio, Φ_{pmix}. These diffusion flames burn with a low-oxygen, high temperature oxidiser stream (reported in Table 1) and, as a result, have very little associated temperature rise, also seen in previous MILD combustion laminar diffusion flame investigations [29]. These flames clearly lie within the MILD regime [1]. As a result of this oxygen deprivation and increased oxidizer stream temperature, the flame stabilizes at leaner mixture fractions than the flames burning with air. Despite a drastically reduced temperature increase associated with combustion (Fig. 7, top), peak X_{OH} values of even the highest diluted flame do not differ greatly from those of conventional flames. This similarity between peak OH values in diluted and conventional diffusion flames supports the experimental finding that the peak OH-PLIF values are not heavily dependent on dilution. Additionally, the width of OH presence in mixture fraction space of diluted and air flames is comparable, if not nearly identical. This supports the finding that, despite burning under MILD

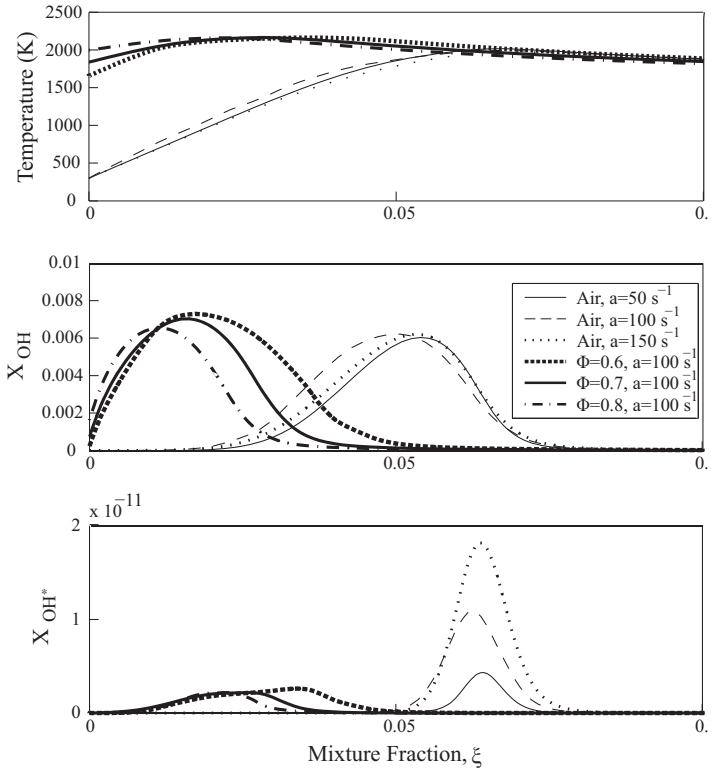

Fig. 7. Calculated temperature, OH mole fraction (X_{OH}), and OH^* excited species mole fraction (X_{OH*}) results in mixture fraction space for laminar non-premixed flames with oxidizer streams of either cold air (marked 'Air') or hot products from a premixed flame (marked with the respective hot product equivalence ratio), at the indicated strain rate, a.

conditions, the investigated CH_4 jet burns in discrete flame fronts comparable to those found in the conventional combustion regime.

By comparing the OH^* emission profiles of the CH_4/air and the MILD flames in Fig. 7, it can be concluded that there is greater distance between the peak OH and peak OH^* locations at MILD conditions than at conventional conditions. In addition, significant OH is evident between the oxidiser (which already contains some OH) and the reaction zone. This provides an explanation for why OH-PLIF signals, indicative of the presence of OH, appear in regions void of OH^* chemiluminescence signal, indicative of heat release (Fig. 5). The use of OH^* chemiluminescence signal as an indicator of heat release in strained non-premixed flames is supported by evaluations of the modified GRI-3.0 mechanism with OH^* and CH^* excited rate constants performed by Panoutsos et al. [23].

Note the much lower OH^* emission of flames burning with hot products compared to flames burning with air, consistent with the experimental adjustment of a higher intensifier gain required to image the presented conditions. Low OH^* emission may be expected in MILD flames, typically known for their low luminosity, an observation which led to the regime's label as "flameless" [1].

4. Conclusions

An experimental study of CH_4 jet flames in a cross-flow of hot combustion products, at times enriched with cold air or diluted with N_2, was performed and supplemented with laminar non-premixed flame calculations. For all cases, the CH_4 jet autoignites and stabilizes as a lifted, strongly bent, turbulent jet flame. OH^* chemiluminescence images show kernels forming and growing. The reaction zone size and shape are significantly affected by X_{O2x} in the range of MILD conditions tested, although the intensity of OH^* emission remains primarily unchanged. By comparing oxidisers with similar temperature and turbulence characteristics, it was found that increased X_{O2x} shifted the jet's ignition and stabilisation further upstream, again supported by images of kernel formation. In all experimental cross-flow cases, regardless of X_{O2x}, thin flame fronts are visible in instantaneous OH-PLIF images, indicating that MILD combustion flames include thin reaction regions. OH-PLIF mean images show the presence of the OH radical in locations where OH^* chemiluminescence mean images do not, suggesting that OH presence in MILD flames does not directly coincide with the flame's primary heat release location as it does in conventional flames. These observations are supported by diffusion flame calculations involving fuel burning in hot combustion products.

Acknowledgements

This work has been partially funded by Rolls Royce Group. We thank Drs. J. Kariuki and P. Dickinson for their assistance in data processing.

References

[1] A. Cavaliere, M. de Joannon, *Prog. Energy Combust. Sci.* 30 (2004) 329–366.
[2] B.B. Dally, A.N. Karpetis, R.S. Barlow, *Proc. Combust. Inst.* 29 (2002) 1147–1154.
[3] P.R. Medwell, P.A.M. Kalt, B.B. Dally, *Combust. Flame* 152 (2008) 100–113.
[4] S.M.M. Najafizadeh, M.T. Sadeghi, R. Sotudeh-Gharebagh, D.J.E.M. Roekaerts, *Combust. Flame* 160 (2013) 2928–2940.
[5] R. Cabra, T. Myhrvold, J.Y. Chen, R.W. Dibble, A.N. Karpetis, R.S. Barlow, *Proc. Combust. Inst.* 29 (2002) 1881–1888.
[6] R. Cabra, J.Y. Chen, R.W. Dibble, A.N. Karpetis, R.S. Barlow, *Combust. Flame* 143 (2005) 491–506.
[7] R.L. Gordon, A.R. Masri, E. Mastorakos, *Combust. Flame* 155 (2008) 181–195.
[8] C.N. Markides, E. Mastorakos, *Proc. Combust. Inst.* 30 (2005) 883–891.
[9] E. Oldenhof, M.J. Tummers, E.H. van Veen, D.-J.E.M. Roekaerts, *Combust. Flame* 157 (2010) 1167–1178.
[10] E.R. Hasselbrink, M.G. Mungal, *J. Fluid Mech.* 443 (2001) 1–25.
[11] E.R. Hasselbrink, M.G. Mungal, *J. Fluid Mech.* 443 (2001) 27–68.
[12] A.R. Karagozian, *Prog. Energy Combust. Sci.* 36 (2010) 531–553.
[13] R.W. Grout, A. Gruber, C.S. Yoo, J.H. Chen, *Proc. Combust. Inst.* 33 (2011) 1629–1637.
[14] D.J. Micka, J.F. Driscoll, *Combust. Flame* 159 (2012) 1205–1214.
[15] M. de Joannon, R. Ragucci, A. Cavaliere, *Atomization Spray* 9 (1999) 153–172.
[16] A.K. Gupta, S. Bolz, T. Hasegawa, *J. Propul. Power* 121 (1999) 209–216.
[17] M. Katsuki, T. Hasegawa, *Proc. Combust. Inst.* 27 (1998) 3135–3146.
[18] J. Kariuki, J.R. Dawson, E. Mastorakos, *Combust. Flame* 159 (2012) 2589–2607.
[19] D.E. Cavaliere, J. Kariuki, *Flow Turbul. Combust.* 91 (2013) 347–372.
[20] B.D. Pratte, W.D. Baines, *J. Hydronaut. Div. ASCE* 92 (1967) 53–64.
[21] Rotexo-Softpredict-Cosilab GmbH and Co. KG Bad Zwischenahn (Germany), Cosilab Collec-tion, Version 3.3.2 (2012).<www.SoftPredict.com>
[22] G.P. Smith, D.M. Golden, M. Frenklach, N.W. Moriarty, B. Eiteneer, M. Goldenberg, C.T. Bowman, R.K. Hanson, S. Song, W.C.J. Gardiner, V. Lissianski, Z. Quin (-). URL: http://www.me.berkeley.edu/gri_mech/.
[23] C. Panoutsos, Y. Hardalupas, A. Taylor, *Combust. Flame* 156 (2009) 273–291.
[24] S.A. Carl, M. Van Poppel, J. Peeters, *J. Phys. Chem. A* 107 (2003) 11001–11007.
[25] R.M.I. Elsamra, S. Vranckx, S.A. Carl, *J. Phys. Chem. A* 109 (2005) 10287–10293.

[26] M. Tamura, P.A. Berg, J.E. Harrington, et al., *Combust. Flame* 114 (1998) 502–514.
[27] G. Sorrentino, D. Scarpa, A. Cavaliere, *Proc. Combust. Inst.* 34 (2013) 3239–3247.
[28] Y. Minamoto, N. Swaminathan, *Combust. Flame* 161 (2014) 1063–1075.
[29] M. de Joannon, P. Sabia, G. Cozzolino, G. Sorrentino, A. Cavaliere, *Combust. Sci. Technol.* 184 (2012) 1207–1218.